Synergistic *MAPT* mutations as a platform to uncover modifiers of tau pathogenesis

M.R. Bryan[1], MF Almeida[2, 4], Carli K. Opland[1], J. McGillion-Moore[1], Hanna Trzeciakiewicz[1], Diamond King[1], Xu Tian[1], Jui-Heng Tseng[1,3], JC Schisler[2], BA Bahr[4], TJ Cohen[1*]
[1]Neurology, University of North Carolina- Chapel Hill, NC
[2] Pharmacology, University of North Carolina- Chapel Hill, NC
[3]School of Life Sciences, Arizona State University- Tempe, AZ
[4]Biotechnology Research and Training Center, University of North Carolina- Pembroke, NC

From the Department of Neurology, UNC Neuroscience Center, University of North Carolina, Chapel Hill North Carolina, 27599

*To whom correspondence should be addressed: Todd J. Cohen: Department of Neurology, University of North Carolina at Chapel Hill, Chapel Hill NC 27599
toddcohen@neurology.unc.edu; Tel. (919) 966-3759; Fax. (919) 843-4576

Keywords*:* aggregation, Alzheimer's disease, FTDP-17, MAPT, posttranslational modification (PTM), heat-shock proteins, Hsp70, organotypic slices, neurodegeneration, tau, tauopathy

---

Abstract

The natively unfolded tau protein is extremely soluble, which poses challenges when modeling neurofibrillary tangle (NFT) pathology in Alzheimer's disease (AD). To overcome this hurdle, we combined P301L and S320F mutations (PL-SF) to generate a rapid and reliable platform to expedite the discovery of factors that modulate tau aggregation. Using this model, we evaluated heat-shock proteins (Hsp), traditionally linked to tau pathology, but whose role in AD remains enigmatic and controversial. In primary neurons, expression of Hsp70, but not Hsc70 or Hsp90, exacerbated tau aggregation. Conversely, lowering of Hsp70 by shRNA or a chaperone-deficient tau mutant (PL-SF-4Δ) reduced tau phosphorylation and abrogated tau aggregation, highlighting Hsp70 as a key driver of tau aggregation. Functionally, mature aggregate-bearing neurons showed deficits in neuronal firing and network communication, while chaperone-binding deficient tau variants displayed reduced tau pathology and restored network properties. This study provides a powerful cell intrinsic model for accelerated tau aggregation, which can be harnessed to identify regulators of tau aggregation as promising therapeutic targets.

Introduction

Aggregation of the microtubule associated protein tau (MAPT), and the formation of insoluble tau inclusion pathology is a hallmark feature of Alzheimer's disease and related neurodegenerative disorders. In contrast to AD, in which tau pathology is comprised of normal wild-type tau proteins, pathogenic disease-causing mutations in the MAPT gene are implicated in familial frontotemporal dementia linked to chromosome 17 (FTDP-17). Over 50 different pathogenic MAPT missense, silent, and intronic mutations have been identified[1].

In many instances, missense mutations generate loss and gain of function phenotypes including altered MT binding and enhanced tau aggregation propensity, which could be directly implicated in prion-like tau spreading that occurs along defined spatial and temporal brain networks.

While familial missense mutations at residue P301 (e.g., P301L and P301S) have been well characterized as aggregate-prone and MT-binding deficient, less is known about nearby mutations within the MT-binding repeat domain (MTBR). Our recent study characterized a panel of FTDP-17 tau mutations spanning this domain and found that the cellular surveillance machinery composed of HDAC6 and associated chaperones (e.g. Hsp70) shows increased binding to two specific mutations within the R3 domain (P301L and S320F), but not others, suggesting these two mutants are conformationally distinct and are more effectively recognized by the quality control machinery that targets tau for degradation[1].

In separate studies, the P301L and S320F mutations were combined into the same full-length tau molecule (termed PL-SF), which generated a surprisingly aggregate-prone conformation leading to an accelerated AD-like tangle pathology, neuroinflammation and memory impairments in mice and rhesus macaques[2–6]. This suggests that PL-SF could potentially be leveraged as an intrinsic, cell-autonomous, and seeding independent model of full-length tau aggregation, which would otherwise be challenging to achieve with full-length tau. In fact, many of the widely used tau biosensor models employ artificial truncated tau mutants comprising only the tau repeat domain, a fragment with questionable relevance to neurons[7]. Once fully characterized, the PL-SF model has obvious benefits including a rapid model of mature tau aggregation and the ability to pursue high-throughput discovery of tau modifiers.

The extent to which tau-bound chaperones such as inducible Hsp70, constitutive Hsc70, and related Hsp90 modulate tau function remains unclear. This debate has obvious therapeutic implications since Hsp inhibitors are in clinical development and have been evaluated in preclinical models of AD[8–13]. However, prior studies have yielded quite contradictory results, since on the one hand Hsp70 facilitates the MC1-positive tau conformation[14], while other studies suggest anti-tau properties in which Hsp70 and Hsc70 mediate tau degradation via autophagy and the ubiquitin proteasome system (UPS)[15,16]. One possible explanation for these discrepancies is the inability to generate mature tau pathology as observed in human AD brains. Adding additional complexity, tau interacts with dozens of chaperone adaptors that may promote or suppress chaperone function directed towards tau[18–21]. Here, we characterized a tau PL-SF model of accelerated tau pathology, which allowed us to interrogate the role of Hsp70 and other chaperones as bona fide modifiers of tau-mediated toxicity and aggregation.

Results

Synergistic familial *MAPT* mutations drive tau phosphorylation and aggregation

We first evaluated tau aggregation in PL-SF expressing immortalized QBI-293 cells. Cells transfected with human T40 (2N4R) wild-type, P301L, S320F, or PL-SF were monitored for RIPA-soluble expression of phosphorylated tau (AT8 and AT100) and cleaved tau (TauC3), two well established markers of tau pathogenesis. Cleaved tau accumulation was only observed in SF or PL-SF. Phosphorylated tau accumulated in

PL-SF expressing cells, more so than WT or either single mutant (**Figure 1 A, B**). Confirming this finding, total tau immunoblotting revealed up-shifted tau protein bands in SF and PL-SF, indicative of tau hyper-phosphorylation. Surprisingly, the single PL mutant appeared hypo-phosphorylated compared to WT or SF mutations. Immunocytochemistry confirmed these findings and revealed Thioflavin S (ThioS) positive SF and PL-SF aggregates, consistent with enhanced tau aggregation (**Supplemental Figure 1, Figure 1C**). Multiple familial missense mutations occur at residues P301 (P301L, P301S, P301T) and S320 (S320F, S320Y). We evaluated a panel of other combination mutants by immunoblotting and immunocytochemistry and found that all double mutants formed phosphorylated, cleaved, and insoluble tau species compared to single tau mutants (**Supplemental Figure 2**). The most consistently insoluble tau species was PL-SF, which we selected for follow-up analysis.

A prior study found that deletion of four key residues in tau (I277/I278 and I308/V309) can abrogate Hsp70 binding[17]. Since the role of Hsp70 in tau pathology remains unclear, we generated a PL-SF mutant in which these four residues were depleted, termed PL-SF 4Δ. In transfected QBI-293 cells, PL-SF 4Δ was nearly completely dephosphorylated and accumulated negligible cleaved tau. PL-SF 4Δ was also downshifted compared to PL-SF, confirming loss of post-translational modifications (**Figure 1D, E**). PL-SF 4Δ showed significantly less phosphorylated (AT8), cleaved (TauC3), and aggregated (ThioS) tau (**Supplemental Figure 3, Figure 1F**). By co-immunoprecipitation, we confirmed that PL-SF 4Δ abrogates the majority of Hsc70 and Hsp70 binding to tau. We did not observe detectable and specific binding to endogenous Hsp90 in our model (**Figure 1G**). We also assessed acetylated-tubulin (ac-tubulin) expression, a readout for microtubule (MT) stability across tau mutants to measure their capacity to modulate MT dynamics. Wild-type tau increased ac-tubulin, as expected, while P301L or S320F were less effective (~30-40%). Consistent with a near-complete loss of MT regulatory function, PL-SF reduced ac-tubulin levels down to the levels of non-transfected cells. Surprisingly, PL-SF 4Δ partly restored tubulin interactions (**Figure 1H, I**).

Impaired chaperone binding alleviates tau pathology in neurons

To validate our findings in neurons, we developed mutant tau lentiviral constructs suitable for high efficiency transduction into mouse primary cortical neurons. Transduced primary neurons were evaluated with a panel of tau mutants including PL-SF. Immunoblotting of neuronal lysates showed that PL-SF tau was again up-shifted and accumulated more phosphorylated tau (**Figure 2A, B).** Unlike cell lines, neurons did not show appreciable tau cleavage (TauC3). Only PL-SF accumulated in the insoluble fraction (**Figure 2C**). PL-SF 4Δ showed a marked reduction in tau phosphorylation and aggregation, suggesting loss of Hsp binding detoxifies tau in neurons as well. In fact, deletion of just two of the Hsp-binding residues (ΔI277/I278 or ΔI308/V309) abrogated tau phosphorylation and aggregation, with residues I308/V309 showing the most dominant effect (**Figure 2A-C**).

By immunocytochemistry in transduced neurons, PL-SF accumulated AT8, MC1, and ThioS positive tau inclusions (**Figure 2D, E**). Both MC1 and AT8 immunoreactive tau was amorphous and globular and accumulated as large varicosities, or swellings, within neurites.

The large globular tau aggregates colocalized with ThioS, supporting tangle-like pathology (**Figure 2F, G**). By transducing neuronal cultures with GFP tagged PL-SF and labeling neurons with a mouse specific tau antibody (monoclonal T49), we observed endogenous mouse tau recruited to PL-SF inclusions, implying that no species barrier exists between human PL-SF aggregates and mouse tau (**Figure 2H**). PL-SF behaved similarly in tau knockout neurons, and therefore endogenous tau is not required for the accumulation of PL-SF pathology in neurons (**Supplemental Figure 4**).

Hsp70 promotes tau hyperphosphorylation and aggregation

To determine whether Hsp70 is a more potent regulator of tau pathology compared to other tau-associated heat shock protein, PL-SF expressing neurons were co-transduced with either HSP70, HSC70, or HSP90. Only Hsp70, but not Hsc70 or Hsp90, exacerbated tau phosphorylation (AT8), which was supported by an appreciable upshift in tau's molecular weight (**Figure 3A, B**) and even a trend towards increased levels of total insoluble PL-SF tau (**Figure 3C, D**). Hsp70 significantly increased AT8, MC1, and ThioS immunoreactivity (**Figure 3E, F**). The effect of Hsp70 appears specific to highly aggregate-prone PL-SF tau, since the P301L single mutant was unaffected **(Supplemental Figure 5).**

Next, we depleted HSP70 in PL-SF transduced neurons. We achieved ~ 50% Hsp70 knockdown using lentiviral shRNA transduction, which did not affect HSC70 expression. Strikingly, HSP70 knockdown led to ~70% decrease in phosphorylated tau (**Figure 4 A, B**) and ~50% decrease in total insoluble tau (**Figure 4C, D**). However, we note that a ~50% decrease in soluble tau was also observed, suggesting Hsp70 depletion also enhances turnover of steady-state tau levels (**Figure 4A, B**). The impact of Hsp70 on tau appears quite specific since knockdown of HSP90 did not alter total or phosphorylated tau (**Supplementary Figure 6**). Overall, our findings highlight Hsp70 as a primary regulator of aggregate-prone tau species in an accelerated PL-SF tau model.

Cell autonomous aggregated tau alters neuronal activity and network synchrony

Given the extensive tau pathology observed in PL-SF transduced neurons, we evaluated any deficits in neuronal activity and connectivity. Electrically active neurons were transduced at DIV18 following an initial multi-electrode array (MEA) recording. Daily recordings were taken for 53 days, and in parallel neurons were immunolabeled at DIV29 and DIV62 to assess the extent of tau pathology.

We evaluated mean firing rate (a measure of overall activity), number of network bursts (a measure of neuronal connectivity), and area under normalized crossed-correlation (a readout for neuronal synchrony). After 15-20 days post lentiviral transduction, PL-SF neurons showed a decline in all three metrics, suggesting loss in neuronal activity and reduced synchronous firing across neuronal networks. The deficits worsened over time, but some neurons continued to fire even past DIV50 (**Figure 5A-C**). Raster plots at DIV54 highlight reduced network firing across MEA electrodes and elongated network firing time (**Figure 5D-F**). PL-SF 4Δ did not exhibit any deficits in any of the activity metrics and showed similar firing patterns compared to wild-type control neurons (**Figure 5A-C**).

The impact of aggregate-prone tau mutants on neuronal firing could represent a direct effect of tau at the synapse. We assessed whether PL-SF accumulated at the post-synaptic density (PSD), a re-

localization thought to coincide with synaptic dysfunction. PSD fractions were biochemically isolated from transduced neurons at DIV18 and probed by immunoblotting for phosphorylated and total tau. PL-SF accumulated in the PSD fraction, an effect that was not observed with PL-SF 4Δ or any single tau mutants (e.g., P301L) (**Figure 5G**). Thus, PL-SF mature tau aggregates accumulate at the PSD and drive synaptic dysfunction. By abrogating Hsp binding, PL-SF 4Δ bypasses these defects.

PL-SF expressing neurons were aged in culture in tandem with MEA cultures to determine tau phenotypes over time. Indeed, aged neurons accumulated dense tau inclusions comprised of phosphorylated, MC1, and ThioS positive tau at DIV29 that became even more intensely labeled by DIV62. All indicators of tau pathology were absent in PL-SF 4Δ expressing neurons at late time points (**Figure 5H**). We also note that Hsp70 began to colocalize with aggregated tau in aged neurons (**Figure 5I**), further supporting aggregation-dependent recruitment of Hsp70.

Cell autonomous tau pathology in organotypic brain slice cultures

To validate our findings in more physiologically relevant brain cultures comprised of both neurons and glia, we transduced adult rat organotypic hippocampal brain slices ex-vivo with either GFP alone, wild-type tau-GFP, PL-SF-GFP, or PL-SF 4Δ-GFP at DIV1 and imaged brain slices after nine weeks in culture **(Figure 6A, B**). Similar to cultured neurons, PL-SF accumulated dense AT8 and MC1 positive inclusions and distinct neuritic puncta, or foci. Most tau pathology preferentially accumulated in the dentate gyrus (DG) and extended though hippocampal CA1 and CA3 regions. In striking contrast, PL-SF 4Δ showed diffuse, non-aggregated neuronal labeling in the DG and far lower levels of pathogenic tau markers, e.g., MC1, AT8 **(Figure 6C, D)**. Therefore, in a multicellular brain model with complete hippocampal architecture, these results suggest that abrogating tau-Hsp binding can confer neuroprotection.

Discussion

Here, we characterized a cell autonomous model of tau aggregation based on the synergistic aggregation of tau missense mutations at residues P301 and S320. Given the accelerated tau aggregation observed within days (in primary neurons), the PL-SF model lends itself readily to the identification of regulators of tau aggregation. Indeed, we leveraged this model to add clarity to a longstanding debate on the role of Hsp70 as a tau modifier. The PL-SF model could help unravel the stepwise generation of tau pathology and provide a more reliable and sensitive system to identify subtle regulators of tau pathogenesis.

Synergistic tau mutants as a model of mature tauopathy

Prior studies have suggested that combining P301L and S320F (PL-SF) can lead to accelerated tau aggregation[2–6] . Here, we expanded on this concept by analyzing the biochemical and histological properties of PL-SF in cells, cortical neurons, and organotypic brain slices. Strikingly, PL-SF tau inclusions appear quite similar to those detected in post-mortem AD brain. Future cryo-EM studies may be needed to better define their ultrastructural properties[18–21] . However, if PL-SF does indeed form AD-like filaments, it may be a preferred model over other individual tau variants (P301S and P301L) that lack mature amyloid structure in culture and mouse models[22,23]. The PL-SF tau variant also accumulated at the post-synaptic density (PSD) and led to functional deficits in neuronal firing and

connectivity (**Figure 5 A-H**), supporting its synaptic toxicity. This rapidly maturing pathology likely allows for faster and more sensitive functional defects.

Exactly how these two mutations (P301L or S320F) synergize to promote tau pathology and drive tau-mediated toxicity is unclear. But we can envision several scenarios.

First, P301L and P301S have been well-characterized to disrupt MT dynamics and promote tau aggregation, but less is known about S320F, linked to Pick's disease. Recently, S320F was found to stabilize a hydrophobic pocket of tau, exposing the ^{306}VQIVYK^{311} amyloid motif and thereby promote aggregation[24]. The combination of these two mutations likely amplifies their proclivity towards β-sheet self-assembly. If true, amyloid-breaking proline mutations within the MTBR would disrupt aggregation, as has been observed with repeat domain aggregation[25–29] .

Second, by extension of its aggregation propensity, PL-SF tau may also be more highly decorated with pathological PTMs than either single tau mutant, driving conformational changes (i.e., MC1). In this study, we only evaluated well-known tau phosphorylation epitopes (AT8, AT100, AT180), but future mass spectrometry approaches could determine the temporal emergence of global tau PTMs (**Figure 2A, B**). For instance, increased PTM complexity could create a vicious cycle leading to further loss of tau-MT binding. One can also envision PTM-induced loss of tau binding to quality control machinery, which typically acts in a compensatory manner to prevents aberrant tau[1]. One example is the surveillance factor HDAC6, which binds and maintains tau in the deacetylated state. Thus, PL-SF could overburden the cellular proteostasis capacity, as suggested for human AD[30–32].

Third, P301L and S320F mutations are also known to dissociate tau from microtubules, which would shift their equilibrium to further concentrate tau pools in the cytosol and facilitate their aggregation. PL-SF drastically reduced acetylated-tubulin levels back down to baseline (i.e., non-tau expressing cells) (**Figure 1 H, I**), suggesting PL-SF is almost completely disassociated from microtubules and therefore primed for aggregation.

Lastly, once formed, we found that neuronal PL-SF tau can recruit endogenous mouse tau (detected by T49 antibody) into tau inclusions (**Figure 2H**), consistent with a prior study showing that human PL-SF-expressing mice (SPAM mice) recruited endogenous mouse tau[5]. PL-SF tau therefore may be more seeding competent, in a species independent manner, which could be leveraged to model tau spreading since it poses several advantages over the use of exogenously added brain-derived AD seeds, (e.g., large-scale production, reliability and reproducibility, and fully intact N-terminal domains). We reiterate that further structural studies are needed to determine whether seeding-competent PL-SF resembles human AD-derived tau.

The role of Hsp70 in tau pathology

We added clarity to the long-standing question of whether Hsp70 modulates tau aggregation, as the prior literature is inconsistent and often highlights contradictory models for tau triage via coordinated Hsp binding. Some studies have found that activation or overexpression of Hsp70 can suppress tau aggregation in vitro, which would intuitively suggest a classical Hsp70 chaperone activity as a suppressor of tau aggregation[15,16,33,34] . Adding additional complexity, while Hsp70 can disassemble tau filaments isolated from human AD brain, this chaperone activity released seeding-competent tau species, suggesting any

protection mediated by Hsp70 may depend on the nature of liberated tau species[35]. In contrast, other studies have shown that Hsp70 depletion or small molecule inhibition (YM-01, JG-23/48) may drive tau clearance[10,12,36–40]. We sought to reconcile these differences in the context of our PL-SF cellular model of tau aggregation.

We initially found that Hsp70 tightly associated with PL-SF tau aggregates in vitro and in cell culture, similar to a previous study[41] (**Figure 5I**). HSP70 overexpression was associated with PL-SF phosphorylation and aggregation, while HSP70 depletion reduced total tau levels, including hyperphosphorylated and aggregated tau species (**Figure 3A-D, Figure 4A-D**). Furthermore, abrogating Hsp70 binding using an Hsp70-binding deficient mutant (PL-SF-4Δ) was also sufficient to suppress tau aggregation (**Figure 1, 2, 5, 6)**. At least in a mature tau aggregation model, these data are consistent with Hsp70 stabilizing a misfolded tau state that can evade proper degradation.

In addition to Hsp70, tau is a substrate for Hsp90, which competes for binding sites within tau's MTBR and is thought to promote CHIP-mediated tau degradation and clearance[42–49]. It is plausible that aggregated tau forms as a consequence of an imbalance in the ratio of Hsp70 vs. Hsp90 binding, which if shifted towards Hsp70 could radically shift tau processing away from degradation towards stabilization of aggregated tau intermediates. In this scenario, Hsp70 depletion or inhibition would facilitate proteasome or autophagic targeting (degradation) by shifting the balance away from tau refolding. Future proteomics studies will be needed to determine whether distinct tau triage complexes emerge temporally in response to tau aggregation. For example, identifying the PL-SF interactome over time in culture may uncover distinct triage stages wherein Hsp70 has shifted from pro-folding to pro-aggregation[50].

We did not observe any effect of Hsc70 on tau aggregation. Though highly homologous, Hsc70 is constitutively expressed at ~30-fold higher levels in the brain compared to the inducible Hsp70 isoform[51]. Hsp70, but not Hsc70, overexpression increased the number of MC1 positive neurons by nearly 3-fold (**Figure 3E, F**). Since Hsp70 is more sensitive to redox signaling (via additional cysteine residue reactivity), its activity may be more tunable under stress conditions[52]. Our data suggests that many variables could dictate how effectively Hsp70 targets tau, which include: 1) the extent of MT-dissociated aggregated tau present, 2) the relative balance and abundance of chaperones and co-chaperones that target and triage tau, and 3) the acute vs. chronic state of disease progression, dictating the efficiency of the cellular proteostasis machinery.

Our study substantiates the view that loss or depletion of Hsp70 could be neuroprotective in the context of the AD brain. Although brain specific HSP70 knockout mice are not available (to the best of our knowledge), Hsp70 inhibition using brain permeable compounds may have therapeutic utility. Though one must consider their dual inhibition of both Hsp70 and Hsc70 (e.g., VER-155008), which could be a confounding issue[10,40,53–55]. Nonetheless, the ability to target the brain "chaperome" to shift tau triage towards a degradative state could have important implications towards the development of tau depletion therapeutics without targeting tau itself[38].

Materials and Methods

Plasmid and lentivirus cloning

To generate the pUltra-T40 WT, PL, PL-SF,

SF, PL/SF-2Δ (277-278), PL/SF-2Δ (308-309), PL/SF-4Δ, HSC70-flag, HSP70-flag, and HSP90-flag constructs, the cDNAs were amplified through PCR and inserted into the pUltra vector using AgeI and SalI restriction endonucleases to replace eGFP in pUltra. pUltra-XeGFP was made by removing eGFP using AgeI and BspEI, creating a blunt end with Klenow before circularizing. pUltra-T40 WT (eGFP), PL/SF (eGFP), and PL/SF-4Δ (eGFP) were created by replacing TDP43 in pUltra TDP43 WT (eGFP) using BspEI and SalI. pUltra was ordered from Addgene (Plasmid #24129). shRNA plasmids against HSP70 (TRCN0000098597, TRCN0000098598) and HSP90 (TRCN0000008491, TRCN0000008494) were ordered from the UNC Lenti-shRNA Core Facility. Primers used for vector construction are in Table 1.

QBI-293 cell culture

QBI-293 (HEK293A) cells (ThermoFisher, #R70507) are commercially available and maintained according to standard protocols. QBI-293 cells were cultured in complete DMEM media (10% fetal bovine serum, 1X L-glutamine, and 1X penicillin/streptomycin). QBI-293 cells were transfected with FuGENE 6 transfection reagent (Promega) to express 2N4R tau constructs for 48 hr. Following transfection, cells were lysed and collected in 1X RIPA buffer [50 mM Tris pH 8.0, 150 mM NaCl, 5 mM EDTA, 0.5% sodium deoxycholate, 1% Igepal CA-630, 0.1% SDS] supplemented with deacetylase, phosphatase and protease inhibitors: 1 mM phenylmethylsulfonyl fluoride (PMSF), 10 mM Nicotinamide (NCA), 1 mM sodium orthovanadate (Na3VO4), 1 mM sodium fluoride (NaF), 0.5 M β-glycerophosphate, 2 μM Trichostatin A (TSA), and protease inhibitor cocktail composed of L-1-tosylamide-2-phenylethylchloromethyl, N-tosyl-L-lysine chloromethyl ketone, leupeptin, pepstatin, and soybean trypsin inhibitor, each at 1 μg/ml.

Primary cortical neuron cell culture

Mouse primary cortical culture was performed in accordance with the University of North Carolina (UNC) Institutional Animal Care and Use Committee (UNC IACUC protocol 24-190). Mouse cortical neurons were dissected and isolated from C57Bl/6 mice (Charles River) at embryonic day 15-16 following lethal isoflurane anesthesia. Following anesthesia, embryos were removed from the pregnant abdominal cavity, washed well with ice-cold 70% ethanol and placed in cold Hanks-buffered balanced salt solution (HBSS). Once rinsed, these embryos were moved to a 10cm dish for dissection. The embryos were then removed from the placental membrane and brains were isolated. The cortex was dissected then moved to Hibernate-E solution (BrainBits) with B27 (Gibco) and Glutamax (ThermoFisher). The cerebral cortices were minced thoroughly with forceps and incubated for 30 minutes at 37 °C in HBSS with 20 U/mL papain (Worthington Biomedical), 1mM EDTA, 0.2mg/mL L-Cysteine, and 5U/mL DNAse (Promega). Cortical tissue was further dissociated in plating media (BrainPhys media (Stemcell), 5% fetal bovine serum, 1X B27 (Gibco), 1X penicillin/streptomycin (Gibco), and 1X Glutamax by triturating the sample using a P1000 micropipette. This suspension was centrifuged for 5 min at 1.5 rcf to pellet the cells. The pellet was then resuspended in plating media and passed through a 40 μm cell strainer. A Countess 3 automated cell counter (Invitrogen) was used to count the cells. Cells were plated in plating media at 600,000 cells/well in 6-well plates or 30,000 cells/well in 96-well plates. The next day (DIV1), plating media was completely aspirated and replaced with fresh neuronal media (BrainPhys media

(Stemcell), B27 (Gibco), 1X penicillin/streptomycin (Gibco), and 1X Glutamax).

Lentiviral production

Lentiviral production was performed by co-transfecting 37.5 mg lentivirus plasmid with 25 mg psPAX2, 12.5 mg VSVG, and 6.25 mg REV plasmids per 15 cm culture plates of Lenti-X 293 T cells (Takara). Three 15 cm plates were used for each lentiviral construct production. Roughly 48 hrs after the transfection, cell culture media was collected and subsequently centrifuged at 2000 rcf for 10 min. Lentiviral particles were purified using a double-sucrose gradient method as follows: supernatants were loaded onto a 70–60% to 30–20% sucrose gradient and centrifuged at 70,000 rcf for 2 hr at 17 °C. The 30–60% fraction containing the viral particles was retrieved, resuspended in PBS, filtered with a 0.45 mm filter flask, loaded onto a 20% sucrose solution, and centrifuged a second time at 70,000 rcf for 2 hr at 17 °C. The supernatants were carefully discarded, and the viral particles in the pellet were resuspended in PBS, aliquoted and stored at −□80 °C.

Lentiviral transductions

Primary neurons were transduced with ~3.0×10^{12} viral particles per mL at DIV4 for most experiments (viruses were added at DIV18 for MEA experiments). If neurons were co-transduced with two viruses, both were added sequentially (each at ~3.0×10^{12} viral particles per mL). For transductions, viruses were added directly to the media in each well (1 µl virus per 2 mL media), followed by gentle rocking by hand to distribute viral particles. The following day, virus-containing media was completely aspirated and replaced with half conditioned media (neuronal media from the same neuron culture) and half fresh neuronal media (BrainPhys (StemCell) with B27 (Gibco), Pen-strep (Gibco), and Glutamax (Gibco)). Every two-three days, half of the neuronal media was discarded and replenished with fresh neuronal media until neurons were collected. Most neurons were collected at DIV10 (7 days after transduction), unless otherwise noted.

Immunoblotting and biochemical analysis

RIPA soluble lysates (250 µl per well of a 6-well plate) collected from QBI-293 and primary cortical neuron were sonicated 20 times on ice, then centrifuged at 15,000 rcf for 20 min at 4 °C. The supernatant was removed from the pelleted material, leaving behind a RIPA insoluble pellet. The RIPA insoluble pellet was washed with 250 µl of RIPA lysis buffer with protease, phosphatase, and deacetylase inhibitors and centrifuged at 15,000 rcf for 20 min at 4 °C. This supernatant was removed and discarded. 75 µl of 1% SDS was added to each pellet then sonicated 20 times at room temperature. These samples were then centrifuged at 15,000 rcf at room temperature. The supernatant from these tubes was removed and stored in separate tubes as the SDS-soluble fraction. The RIPA and SDS-soluble supernatants were then mixed with 6X loading dye with DTT and boiled at 98 °C for 10 min in a PCR thermocycler (BioRad). Samples were run and resolved via SDS-PAGE on 4–20% gradient gels (BioRad). Gels were transferred to iBlot 2 Midi nitrocellulose membranes using the iBlot 2 (Invitrogen) following the standard P0, 7-min settings. Following transfer, membranes were blocked with 2% milk in 1X TBS for 30 min and then incubated with primary antibody overnight at 4 °C on a rocker. The next day, membranes were incubated with HRP-conjugated anti-mouse or anti-rabbit antibodies (1:1000) for 1-2 hr at room temperature. Blots were developed with

ECL Western Blotting substrate (Cytiva, Amsterdam) and imaged on a GE ImageQuant LAS4000.

Immunocytochemistry

Immunocytochemistry experiments were performed using QBI-293 cells or cortical primary neurons plated on poly-D-lysine (PDL)-coated 96-well plates. Following either plasmid transfection (48 hr) or lentiviral transduction (7 days unless otherwise stated), cells were washed once in PBS, immediately fixed in 4% paraformaldehyde for 15 min, then washed once more with PBS. Following fixation, cells were then permeabilized with permeabilization buffer (0.2% Triton X-100 (Sigma) in PBS) for 20 min then blocking buffer (4% normal goat serum in PBS with 0.05% Tween 20) for 1 hr. Primary antibodies were added in blocking buffer and incubated overnight on a rocker at 4 °C. The following day, cells were washed 3X in PBS with 0.05% tween 20 and incubated with Alexa 488, Alexa 594, or Alexa 647 conjugated secondary antibodies at 1:1000 and DAPI for 1 hr. Cells were then washed 3X in PBS with 0.05% Tween 20. Cells were then imaged using an EVOS M7000 automated microscope with EVOS 20X objective (Invitrogen AMEP4982) and 40X objectives (Invitrogen AMEP4754) and DAPI, GFP, Texas Red, and Cy5 light cubes. Note: Some representative images were artificially brightened or contrasted in Microsoft PowerPoint or Celleste 5.0 and 6.0 software (Invitrogen) to aid visualization. Any panels assessing the same set of conditions were brightened to identical levels. Images were not manipulated prior to quantification.

Antibodies

The following primary antibodies were used in this study: AT8 (ThermoFisher Scientific-MN1020), AT100 (ThermoFisher Scientific MN1060), AT180 (ThermoFisher Scientific MN1040), TauC3 (ThermoFisher Scientific-AHB0061), T49 mouse tau (Millipore-MABN827), Tau12 (Millipore, MAB2241, 1:1000), Tau5 (AHB0042), Hsp70 used for immunoblotting (Enzo- ADI-SPA-810-D), Hsp70 used for immunoblotting and immunocytochemistry (Cell Signaling Technologies- 4872), Hsc70 1B5 (ADI-SPA-815-F), Hsp90 16F1 (Enzo- adi-spa-835), Total tau rabbit polyclonal- formerly K9JA (DAKO, A0024 1:2000), GAPDH 6C5 (Millipore- MAB374), ac-tubulin (Sigma T7451), alpha tubulin (Sigma, T9026), Anti-FLAG M2 (Sigma, F1804, 1:2000), GFAP (Dako, 20334). The MC1 antibody was kindly shared by Dr. Peter Davies. Quantification of immunoblotting was measured by ImageStudio Lite Version 5.2.

Co-immunoprecipitation reactions

All co-immunoprecipitations were performed in QBI-293 cells transfected with plasmids expressing 2N4R wild-type, P301L, P301L/S320F, and P301L/S320F 4Δ for 48 hours prior to collection. Each well of a 6-well plate was used as separate conditions. Cells were collected in 250 µl RIPA buffer with protease, phosphatase, and deacetylase inhibitors prior to co-immunoprecipitation. Lysates were immediately rotated on a wheel for 30 minutes at 20 rpm at 4 ^{o}C. Lysates were then centrifuged at 15,000 rcf for 15 min at 4 ^{o}C. Supernatants were removed and 40 µl were kept as input. The remaining supernatant was pre-cleared with 50 µl of Protein A/G PLUS-Agarose beads (Santa Cruz, sc2003) for 30 min at 4 ^{o}C. Lysates were centrifuged for 1 min at 1,500 rcf, and the supernatant was removed. The volume of each reaction was brought to 500 µl of RIPA buffer with inhibitors. 8 µl of tau5 antibody was added to each reaction, then 75 µl of agarose protein A/G beads. Lysates were rotated on

a wheel at 20 rpm at 4 ^{o}C overnight. The following day, lysates were centrifuged at 1,500 rcf for 5 minutes. Most of the supernatant was carefully removed, followed by washing with 500 µl of RIPA buffer with inhibitors, and lysates were centrifuged at 1,500 rcf for 5 minutes. This wash was repeated four times. After the final wash, loading dye with DTT was directly added to the beads and heated for 10 minutes at 98 ^{o}C with intermittent mixing. These were centrifuged for 30 seconds at 1,500 rcf prior to storage at -80 ^{o}C.

HSP70 and HSP90 shRNA knockdown

All shRNAs were obtained from UNC Lenti-shRNA core facility and cloned into the pUltra vectors. Sequences: HSP70 shRNA: GCAGGTGAACTACAAGGGCGA; eGFP control shRNA: TACAACAGCCACAACGTCTAT (Y145 to Y151 residues of eGFP). HSP70 shRNAs were added to the neuron culture four days after transduction with tau lentiviruses at a titer of ~3.0x10^{12} viral particles per mL. Media was half exchanged for fresh neuronal media every two days. After an additional four days in culture, primary neurons lysates were collected for experiments. We noted significant toxicity and cell death after more than 4 days in culture with HSP70 shRNAs. HSP90 shRNAs were applied for 7 days in culture (~3.0x10^{12} viral particles per mL) prior to collection for experiments and were not overtly toxic.

Multi-electrode array recordings and analysis

Following dissection, primary mouse cortical neurons were directly plated onto poly-D lysine coated 24-well BioCircuit MEA plates (Axion Biosystems). A 10 µl droplet of neurons at a concentration of 16,000,0000 neurons/mL was added directly to the center of each well. Neurons were incubated at 37°C for 1 hr then 250 µl of plating media (BrainPhys media (Stemcell), 5% fetal bovine serum, 1X B27 (Gibco), 1X penicillin/streptomycin (Gibco), and 1X Glutamax) was carefully added to each well in a circular motion. Following another 1-hour incubation, another 250 µl of plating media was added to each well (total volume = 500 µl). The following day, ~90% of plating media was aspirated and fresh neuronal (BrainPhys media (Stemcell), B27 (Gibco), 1X penicillin/streptomycin (Gibco), and 1X Glutamax) media was added to each well. Half of the media was exchanged for fresh neuronal media every two days. At DIV18, neurons underwent an initial, 10-minute pre-recording using the Axion Maestro Edge (Axion Biosystems) and AxIS Navigator software (Axion Biosystems). Immediately following this recording, neurons were transduced with lentiviruses at ~3.0x10^{12} viral particles per mL (four replicate wells per condition). The following day, neuronal activity was recorded for 10 minutes, then lentivirus-containing neuronal media was completely replaced with half fresh neuronal media and half conditioned neuronal media from the same culture. Neurons were recorded almost every day for 10 minutes and half of the neuronal media was replaced every 2-3 days after recording until DIV71 (day 53 of recording). Post-hoc analysis was performed using the NeuralMetricTool (Axion Biosystems) using default analysis options. Data was exported into Microsoft Excel, then graphed via GraphPad Prism 10 for statistical analyses and graphing. Raster plots were generated from the same data using the AxIS Metric Plotting Tool. 96 well plates were plated at the same time using the same primary neurons, underwent identical media changes, and were used for immunocytochemistry at DIV29 and DIV62 in Figure 5.

Post-synaptic density isolation

Primary mouse cortical neurons from wild-type C57/BL6 mice were plated on poly-D-lysine coated 6-well plates at 600,000 cells/well. Neurons were treated with lentivirus at DIV4 (1 6-well plate per condition) and half-fed every two days until DIV14. At DIV14, neurons were rinsed in cold PBS and all 6-wells of each plate were collected in a total of 900 µl of homogenization buffer (320 mM sucrose, 5 mM sodium pyrophosphate, 1 mM EDTA, 10 mM HEPES pH 7.4) with protease/phosphatase inhibitor cocktail 200 nM okadaic acid, 1 mM orthovanadate, 1X protease inhibitor cocktail (Roche). Neuronal lysates were homogenized by passing the lysate 12 times using a 26g needle. 70 µl of lysate was kept and stored as whole cell lysate. The remaining lysate was centrifuged at 1,000 g for 10 min at 4°C *to* generate pelleted nuclear fraction (P1) and supernatant fraction (S1). The S1 fraction was centrifuged at 15,000 g for 20min at 4°C to generate the membrane/crude synaptosome pelleted fraction (P2) and cytosolic supernatant fraction (S2). The P2 fraction was resuspended in 500 µl of ultrapure H_20 with protease/phosphatase cocktail. 20 µl of 100 mM HEPES was added to the 500 µl of suspension to yield 4 mM HEPES pH 7.4. These samples were then spun on a wheel for 30 min at 4°C then centrifuged for 20 min at 4°C at 25,000 g using a Sorvall mTX 150 ultracentrifuge (Thermo Scientific) to generate pelleted synaptic fraction (LP1) and supernatant fraction (LS2). The LP1 pellet was resuspended in 250 µl mM HEPES pH7.4 using repeated trituration with a micropipette. This was then mixed with 250 µl of 1% Triton X-100 with protease/phosphatase cocktail and spun on a wheel for 10 min at 4°C. This was then centrifuged in Sorvall mTX 150 ultracentrifuge (Thermo Scientific) at 32,000 g for 20 min at 4°C. This pellet was resuspended in 80 µL of 50 mM HEPES pH7.4 using micropipette trituration to yield the PSD fraction. Only total homogenate and PSD fraction were processed and analyzed by SDS-PAGE.

Imaging quantification

All immunocytochemistry (aside from organotypic slice cultures) quantification was performed using Celleste 5.0 and 6.0 software (Invitrogen). The number of inclusions were counted using the count/size function. Inclusions were manually segmented based on intensity (Segment: Manual) and size (Region: Area) thresholds for each tau probe (e.g. AT8, MC1, ThioS). These threshold settings were then applied to all images used for that specific experiment, automatically batched processed using a segment-count-export macro generated in Celleste, then exported to Microsoft Excel for subsequent analysis.

Hippocampal slice cultures

Sprague-Dawley rats (Charles River Laboratories, Wilmington, MA) were housed and maintained in accordance with the recommendations from the Guide for the Care and Use of Laboratory Animals from the National Institutes of Health, and in accordance with an approved protocol from the Institutional Animal Care and Use Committee of the University of North Carolina-Pembroke. Brain tissue from postnatal 12-day-old rats was rapidly prepared and hippocampi positioned on a McIlwain tissue chopper for assembling slices for interface cultures as previously described[56,57]. Three-dimensional organotypic cultures of specific brain regions are well known for studying different types of physiologies and pathogenic processes[58–60]. Transverse hippocampal slices (400-µm thickness) were immediately placed in ice-cooled-buffer

solution (pH 7.2) then transferred in groups of eight to nine onto the Biopore membrane of culture inserts (Millipore, Billerica, MA). The media below the culture inserts contained 50% basal medium eagle (Sigma-Aldrich, St. Louis, MO), 25% Earle's balanced salts (Sigma-Aldrich), 25% horse serum (Gemini Bio-Products, Sacramento, CA), and defined supplements as previously described[61]. The media were initially changed 24 hours after the slicing procedure, followed by subsequent changes every 3-4 days. The cultivated hippocampal slices were maintained under conditions of a 5% CO2-enriched atmosphere at a constant temperature of 37°C for a duration of nine weeks.

Lentiviral infection of organotypic cultures

Lentiviruses expressing GFP or GFP-tagged tau variants (wild-type, PL-SF, and PL-SF 4Δ tau). For each condition, 1.5 µl of lentivirus were applied onto the surface of individual organotypic slices (~7.5×10^{12} viral particles per slice) approximately 3 hours after the placement of the slices on Millipore inserts. Following a nine-week incubation period in vitro, both the infected organotypic slices and their corresponding controls were fixed with 4% PFA for 3-4 hours. Subsequently, the slices were rinsed multiple times with PBS and stored in PBS at 4 ºC.

Immunofluorescence staining and imaging of organotypic cultures

The fixed organotypic hippocampal explants underwent permeabilization in PBS containing 0.5% Triton-X100 for 30 minutes. Following this, the slices were blocked with a solution of 5% BSA in PBS containing 0.1% Triton-X100 for 90 minutes at room temperature. Subsequently, the organotypic slices were incubated for 48 hours at 4 ºC with primary antibodies targeting AT8 (1/400; ThermoFisher Scientific- MN1020) or MC1 (1/400; Dr. Peter Davies, diluted in a solution of 3% BSA containing 0.1% Triton-X100. Next, brain explants were washed 3-4 times with PBS containing 0.1% Triton-X100 and then exposed to Goat anti-mouse IgG Alexa-FluorTM 568 (ThermoFisher, Waltham, MA) for 120 minutes at room temperature. Following this incubation, the organotypic slices were rinsed three times with PBS containing 0.1% Triton-X100. During the second wash, NucBlue stain (Invitrogen, MA, USA) was introduced to the PBS to promote DAPI nuclear staining. Subsequently, the slices were rinsed in PBS and were mounted onto glass slides, covered by 1.5 mm coverslips, using ProlongTM diamond antifade mountant (Thermo Fisher Scientific, NC, USA). Immunofluorescence images were captured with Andor Dragonfly spinning disk confocal using the Zyla Plus 4.2MP sCMOS (Oxford Instruments, Abingdon, United Kingdom). Image our blinded processed adopting the equal adjust using the Imaris Multidimensional visualization and analysis software (Schlieren-Zurich, Switzerland).

Statistical analysis

GraphPad Prism 10 software was used for all statistical analyses. Results were polled from a minimum of n=3 independent experiments and presented as average ± standard error of the mean (SEM).

Acknowledgements
Support for this work was provided by National Institutes of Health (NIH) grants F32AG072826 (MRB) and R01AG068063 (TJC), Duke/UNC Alzheimer's Disease Research Center grant (NIAP30AG072958), Alzheimer's Association grants AARG-22-924321 (TJC) AARF22926617 (JHT), and CurePSP grant 656-2018-06 (TJC). The Andor Dragonfly microscope was funded with support from National Institutes of Health grant S10OD030223. We would also like to thank Kinsley Adams for her expertise and assistance with the hippocampal organotypic slice cultures. The content is solely the responsibility of the authors and does not necessarily represent the official views of the National Institutes of Health.

Conflict of interest
The authors declare that they have no conflicts of interest with the contents of this article.

Author Contributions
MRB designed and performed most experiments. MA, JS, and BB designed and carried out ex vivo organotypic slices experiments and imaging. CO assisted with co-immunoprecipitation experiments, post-synaptic density preparations, and immunohistochemistry protocols. JMM assisted with multi-electrode array recordings and analyses. XT prepared all plasmid and lentiviral constructs for all experiments. DK and HT designed and performed the QBI293 experiments comparing various P301 and S320 tau mutants. MRB and TJC prepared the manuscript and figures. TJC directed and supervised the study. All authors consented and contributed to the final version of the manuscript.

Figure Legends

Figure 1: Abrogation of tau binding to heat shock proteins (Hsp) alleviates tau pathology in a PL-SF tau aggregation model.
A) Representative immunoblots (RIPA fraction) of QBI-293 cells transfected with 2N4R WT, P301L, S320F, or P301L-S320F tau. **B)** Immunoblot quantification of total tau, p-tau (AT8 and At100), and cleaved tau (TauC3) in RIPA fraction. N=4 per condition; **C)** Immunocytochemistry quantification of QBI-293 cells transduced with WT, P301L, S320F, or PL-SF tau labeled with AT8, TauC3, or ThioS. N=48 FOVs per condition. Representative images found in Supplemental Figure 1. **D)** Representative immunoblots (RIPA fraction) of QBI-293 cells transfected with 2N4R P301L-S320F tau or P301L-S320F 4Δ (deletion of I277/278, I308/V309 residues). *AT100 was run on a separate blot with the exact same lysates to improve detection. **E)** Immunoblot quantification of total tau, p-tau (AT8 and AT100), and cleaved tau (TauC3) in RIPA soluble fractions. N=3 per condition. **F)** Immunocytochemistry quantification of QBI-293 cells transduced with 2N4R PL-SF or PL-SF 4Δ tau labeled with AT8, TauC3, or ThioS. N=16 FOVs per condition. Representative images found in Supplemental Figure 3. **G)** Co-immunoprecipitation of QBI-293 cells transfected with WT, P301L, PL-SF, or PL-SF 4Δ tau. Tau5 antibody was used to IP tau and immunoblots were probed with total tau (rabbit polyclonal) and Hsp70, Hsc70, and Hsp90 antibodies. **H)** Representative immunoblots of QBI-293 cells transfected with 2N4R tau variants and probed with acetyl-tubulin and total alpha-tubulin antibodies. Note: Acetyl tubulin and alpha tubulin blots were run separately with the same lysates to improve detection. **I)** Quantification of acetyl-tubulin across all 2N4R tau variants. -- line signifies separate sets of transfections in panel I and J. N=4 per condition; *= p-value significant by one-way ANOVA. Control= empty plasmid vector (pcDNA3.1)**.**

Figure 2: Development and characterization of a PL-SF tau aggregation model in primary cortical neurons.
A) Representative RIPA-soluble immunoblots of DIV10 primary cortical neurons transduced with lentiviruses expressing 2N4R WT, P301L, S320F, P301L-S320F, or PL-SF 2Δs (R2 and R3) and 4Δ tau variants. **B)** Quantification of AT8, AT100, AT180, and total tau immunoblots in primary cortical neurons (RIPA fraction). N=3 per condition; *= p-value significant by one-way ANOVA. **C)** Representative SDS-soluble immunoblots of DIV10 primary cortical neurons transduced with lentiviruses expressing 2N4R WT, P301L, S320F, P301L-S320F, or PL-SF 2Δ and 4Δ tau variants. N=2 for control, WT, and P301L; N=3 for other variants. **D)** Representative immunocytochemistry images of 2N4R tau variants labeled with AT8 (p-tau), MC1 (conformational tau), ThioS (aggregated tau) in GFP. Scale bar= 125 µm. **E)** Quantification of the number of AT8, MC1, and ThioS inclusions in PL-SF and PL-SF 2Δ (R2 and R3) and 4Δ variants. N=12-24 FOVs per condition. *= significant by one-way ANOVA. **F, G)** Representative immunocytochemistry images of PL-SF tau displaying colocalization between F) AT8 (p-tau) or G) MC1 (conformational tau) with ThioS (aggregated tau). Scale bar= 50um. **H)** Representative immunocytochemistry of PL-SF GFP colocalized with T49 tau (mouse-specific). Scale bar= 125 µm. Control= empty viral vector (pUltra)**.**

Figure 3: Hsp70 exacerbates tau hyperphosphorylation and aggregation.
A) Representative immunoblots of 2N4R PL-SF tau co-transduced with HSP70, HSC70, and HSP90 in DIV10 primary cortical neurons (RIPA fraction). **B)** Quantification of AT8 (p-tau),

total tau (rabbit polyclonal), or Hsp70, Hsc70, Hsp90 (FLAG-tagged) in the RIPA fraction. N=6 per condition. *= p-value significant by one-way ANOVA. **C)** Representative immunoblots of 2N4R PL-SF tau co-transduced with HSP70, HSC70, and HSP90 in DIV10 primary cortical neurons (SDS fraction). **D)** Quantification of AT8 (p-tau), total tau (rabbit polyclonal) in the SDS fraction. N=6 per condition. ns= p-value is not significant by one-way ANOVA. **E)** Representative immunocytochemistry images of primary cortical neurons co-transduced 2N4R PL-SF tau and HSP70, HSC70, or HSP90 labeled with AT8, MC1, Tau12 (RFP) or ThioS (GFP). Scale bar= 125 µm. **F)** Quantification of MC1, AT8, and ThioS positive inclusions in primary cortical neurons co-transduced 2N4R PL-SF tau and either HSP70, HSC70, or HSP90. n=12 FOVs per condition. *= p-value significant by one-way ANOVA. Control= empty viral vector (pUltra)**.**

Figure 4: Reducing HSP70 can suppress tau hyper-phosphorylation and aggregation.
A) Representative immunoblots of 2N4R PL-SF tau co-transduced a shRNA against HSP70 in DIV10 primary cortical neurons (RIPA fraction). **B)** Quantification of AT8 (p-tau), total tau (rabbit polyclonal) and endogenous Hsp70 and Hsc70 in the RIPA fraction. N=3. **C)** Representative immunoblots of 2N4R PL-SF tau co-transduced a shRNA against HSP70 in DIV10 primary cortical neurons (SDS fraction). **D)** Quantification of AT8 (p-tau), total tau (rabbit polyclonal) in the SDS fraction. N=3. *= p-value significant by one-way ANOVA. Control= empty viral vector (pUltra)**.**

Figure 5: Mature tau aggregates cause functional deficits in neurons that can be reversed by abrogating tau-Hsp binding.
A-C) Quantification of neuronal activity comparing PL-SF to PL-SF 4Δ across 53 days of multi-electrode array recording starting at DIV18 following initial pre-recording. A) Mean firing rate-activity B) Number of network bursts- connectivity C) Area under normalized cross-correlation-synchrony. N=4 replicate wells per condition. *= p-value significant by one-way ANOVA. **D-F)** Representative raster and network burst plots at DIV54 (day 36 of recording) comparing empty control (pUltra) to PL-SF and PL-SF 4Δ. D) Number of network bursts across electrodes over time (pink lines) E) number of spikes across electrodes over time F) Average number of spikes per network burst over time. **G)** Representative immunoblot of isolated post synaptic density (PSD) in DIV18 primary cortical neurons transduced with lentiviruses expressing P301L, PL-SF, or PL-SF 4Δ. Immunoblot was probed with PSD95, AT8 (p-tau), and rabbit polyclonal tau (total tau). **H)** Representative 20X immunocytochemistry images of primary cortical neurons comparing empty vector control (pUltra) to PL-SF and PL-SF 4Δ tau variants at DIV29 and DIV62. Neurons were labeled with ThioS (aggregated tau), MC1 (conformational tau), AT8 (p-tau), and Tau12 (total tau) in GFP. Tau12 was co-labeled with GFAP (RFP) to label astrocytes. Scale bar= 125 µm. **I)** Representative immunocytochemistry images of primary cortical neurons comparing PL-SF and PL-SF 4Δ at DIV29. Neurons were labeled with endogenous Hsp70 (GFP), MC1 or AT8 (RFP), and DAPI (BFP). Scale bar= 50 µm. Control= empty viral vector (pUltra)**.**

Figure 6: Abrogating tau-Hsp binding suppresses tau pathology in three-dimensional organotypic hippocampal slice cultures. Rat hippocampal slices were processed for immunocytochemistry after 9 weeks in culture following lentiviral infection of eGFP empty vector control, wild-type tau, PL-SF tau, and PL-SF 4Δ. **A, B)** Immunocytochemistry of the

entire hippocampal slice following labeling of reveal sufficient expression of PL-SF and PL-SF 4Δ lentiviruses (GFP). Left- AT8 staining; Right- MC1 staining. CA1, CA3, and DG regions are labeled in white font. White boxes denote magnified images in panel C, D. Scale bar= 500 µm. **C, D)** Representative immunocytochemistry images of C) AT8 and D) MC1 labeled in RFP for empty vector control, wild-type tau, PL-SF tau, and PL-SF 4Δ taken from the dentate gyrus (DG) region of the hippocampal slice culture (inset white boxes from A, B). Scale bar= 100 µm.

Supplemental Figure 1: Accelerated PL-SF aggregation compared to single tau mutants in immortalized cell lines. A) Representative immunocytochemistry images from QBI-293 cells expressing empty vector (pcDNA) or WT, PL, SF, and PL-SF tau variants. Cells were labeled with AT8 (p-tau) or TauC3 (C-terminal cleaved tau) with rabbit polyclonal tau (total tau) and ThioS with Tau12 (human tau). Quantification of images is found in Figure 1C. Control= empty plasmid vector (pcDNA3.1). Scale bar= 125 µm.

Supplemental Figure 2: Immunoblotting analysis of a panel of P301 and S320 single and combination mutants. A-G) Quantification of AT8, MC1, TauC3, and ThioS immunocytochemistry in QBI-293 cells expressing various P301 and S320 mutants alone or in combination. Panels E-G are subsets of data from A-C to perform additional comparisons among combinatorial mutants. Representative images not shown. Error bars= SEM. *= significant difference by one-way ANOVA. **H)** Representative immunoblots from QBI-293 cells expressing wild-type, P301S/S320F, P301T/S320F, and P301L/S320F tau variants. RIPA (soluble) and urea (insoluble) fractions were analyzed by immunoblotting for p-tau epitopes (AT8, AT180, AT270, p-396) and total tau (rabbit polyclonal). **I, J)** Quantification of RIPA soluble and urea (insoluble) fractions. Error bars= SEM. *= significant difference by one-way ANOVA.

Supplemental Figure 3: Abrogating Hsp binding using the PL-SF 4Δ variant suppresses the accumulation of pathological tau. Representative immunocytochemistry images from QBI-293 cells expressing tau PL-SF and PL-SF 4Δ tau variants. Cells were probed with AT8 (p-tau), TauC3 (C-terminal cleaved tau) with rabbit polyclonal tau (total tau), and ThioS with Tau12 (human tau). Quantification of images is found in Figure 1F. Control= empty plasmid vector (pcDNA3.1)**.** Scale bar= 125 µm.

Supplemental Figure 4: Mature PL-SF aggregates emerge similarly in either wild-type or tau knockout neurons lacking endogenous mouse tau. A) RIPA (soluble) immunoblot of wild-type tau and tau knockout neurons probed with p-tau (AT8, AT180, AT100) and total tau (rabbit polyclonal). **B)** SDS (insoluble) immunoblot of wild-type tau and tau knockout neurons probed with p-tau (AT8) and total tau (rabbit polyclonal). **C)** Representative immunoblotting images of wild-type, P301L, S320F, and P301L/S320F tau variants in wild-tau-expressing or tau knockout neurons. Neurons were labeled with AT8 (GFP) and rabbit polyclonal total tau (RFP), MC1 (GFP), or ThioS (GFP) and Tau12 (RFP). Scale bar= 125 µm. Control= empty viral vector (pUltra)**.**

Supplemental Figure 5: Overexpression of HSP70 in P301L-expressing neurons does not promote tau phosphorylation or aggregation. A) RIPA (soluble) immunoblot of primary neurons following 1-week of lentiviral co-transduction with P301L tau and HSP70. Blot was probed with p-tau (AT8), total tau (rabbit polyclonal), and M2 FLAG (Hsp70-FLAG). **B)** SDS

(insoluble) immunoblot of primary neurons was unable to detect insoluble tau species with total tau antibody (rabbit polyclonal). Control= empty viral vector (pUltra)**.**

Supplemental Figure 6: HSP90 depletion does not alter phosphorylated or aggregated PL-SF tau. A) RIPA (soluble) immunoblot of primary neurons probed with p-tau (AT8) and Hsp90 following 1-week of lentiviral HSP90 knockdown with two shRNAs (called TRC91 and TRC94). **B)** SDS (insoluble) immunoblot of primary neurons probed with p-tau (AT8) and total tau (rabbit polyclonal) following 1-week of lentiviral HSP90 knockdown. **C)** Quantification of AT8 and Hsp90 in the RIPA fraction. Error bars= SEM. **D)** Quantification of AT8 and total tau (rabbit polyclonal) in SDS fraction. *Note: Only TRC94, and not TRC91, HSP90 shRNA was able to reduce Hsp90 expression.

Table 1: Primers used for vector construction

Primer	Sequence
d277-278F	AATAAGAAGCTGGATCTTAGCAACGTC
d277-278R	CTGCACCTTCCCGCCTCC
d308-309F	TACAAACCAGTTGACCTGAGCAAG
d308-309R	TTGCACACTGCCGCCTCC
Tau F	CCGACCGGTGCCACCATGGCTGAGCCCCGCCAG
Tau R	CGCGTCGACTCACAAACCCTGCTTGGCCAGG
HSP70-F	GCGACCGGTGCCACCATGGATTACAAGGATGACGACGATAAGATGGCCAAAGCCGCGGCGATCG
HSP70-R	TCGGTCGACCTAATCTACCTCCTCAATGGTGGGGCC
HSC70-F	GCGACCGGTGCCACCATGGATTACAAGGATGACGACGATAAGATGTCCAAGGGACCTGCAGTTGG
HSC70-R	TCGGTCGACATCAACCTCTTCAATGGTGGGCCC
Hsp90-F	GCGACCGGTGCCACCATGGATTACAAGGATGACGACGATAAG
Hsp90-R	GCGGTCGACGCTAGTCTACTTCTTCCATGCGTGATGTG

References

1. Trzeciakiewicz, H. *et al.* An HDAC6-dependent surveillance mechanism suppresses tau-mediated neurodegeneration and cognitive decline. *Nat Commun* **11**, 5522 (2020).
2. Koller, E. J. *et al.* Combining P301L and S320F tau variants produces a novel accelerated model of tauopathy. *Hum Mol Genet* **28**, 3255–3269 (2019).
3. Strang, K. H. *et al.* Distinct differences in prion-like seeding and aggregation between tau protein variants provide mechanistic insights into tauopathies. *J Biological Chem* **293**, 2408–2421 (2017).
4. Croft, C. L. *et al.* rAAV-based brain slice culture models of Alzheimer's and Parkinson's disease inclusion pathologies. *J Exp Medicine* **216**, 539–555 (2019).
5. Xia, Y. *et al.* Pathogenic tau recruits wild-type tau into brain inclusions and induces gut degeneration in transgenic SPAM mice. *Commun Biology* **5**, 446 (2022).
6. Beckman, D. *et al.* Temporal progression of tau pathology and neuroinflammation in a rhesus monkey model of Alzheimer's disease. *Alzheimer's Dement.* **20**, 5198–5219 (2024).
7. Kaniyappan, S. *et al.* FRET-based Tau seeding assay does not represent prion-like templated assembly of Tau fibers. *Biorxiv* 2020.03.25.998831 (2020) doi:10.1101/2020.03.25.998831.
8. Xu, P. *et al.* Allosteric inhibition of HSP70 in collaboration with STUB1 augments enzalutamide efficacy in antiandrogen resistant prostate tumor and patient-derived models. *Pharmacol. Res.* **189**, 106692 (2023).
9. Li, X. *et al.* Analogues of the Allosteric Heat Shock Protein 70 (Hsp70) Inhibitor, MKT-077, As Anti-Cancer Agents. *Acs Med Chem Lett* **4**, 1042–1047 (2013).
10. Miyata, Y. *et al.* Synthesis and Initial Evaluation of YM-08, a Blood-Brain Barrier Permeable Derivative of the Heat Shock Protein 70 (Hsp70) Inhibitor MKT-077, Which Reduces Tau Levels. *Acs Chem Neurosci* **4**, 930–939 (2013).
11. Moradi□Marjaneh, R., Paseban, M. & Marjaneh, M. M. Hsp70 inhibitors: Implications for the treatment of colorectal cancer. *IUBMB Life* **71**, 1834–1845 (2019).
12. Abisambra, J. *et al.* Allosteric Heat Shock Protein 70 Inhibitors Rapidly Rescue Synaptic Plasticity Deficits by Reducing Aberrant Tau. *Biol Psychiat* **74**, 367–374 (2013).
13. Biamonte, M. A. *et al.* Heat Shock Protein 90: Inhibitors in Clinical Trials. *J. Med. Chem.* **53**, 3–17 (2010).
14. Jinwal, U. K. *et al.* Hsc70 Rapidly Engages Tau after Microtubule Destabilization*. *J Biol Chem* **285**, 16798–16805 (2010).
15. Kundel, F. *et al.* Hsp70 Inhibits the Nucleation and Elongation of Tau and Sequesters Tau Aggregates with High Affinity. *ACS Chem. Biol.* **13**, 636–646 (2018).
16. Patterson, K. R. *et al.* Heat Shock Protein 70 Prevents both Tau Aggregation and the Inhibitory Effects of Preexisting Tau Aggregates on Fast Axonal Transport. *Biochemistry* **50**, 10300–10310 (2011).
17. Sarkar, M., Kuret, J. & Lee, G. Two motifs within the tau microtubule-binding domain mediate its association with the hsc70 molecular chaperone. *J Neurosci Res* **86**, 2763–2773 (2008).

18. Scheres, S. H., Zhang, W., Falcon, B. & Goedert, M. Cryo-EM structures of tau filaments. *Curr. Opin. Struct. Biol.* **64**, 17–25 (2020).
19. Fitzpatrick, A. W. P. *et al.* Cryo-EM structures of tau filaments from Alzheimer's disease. *Nature* **547**, 185–190 (2017).
20. Tarutani, A. *et al.* Cryo□EM structures of tau filaments from SH□SY5Y cells seeded with brain extracts from cases of Alzheimer's disease and corticobasal degeneration. *FEBS Open Bio* **13**, 1394–1404 (2023).
21. Arakhamia, T. *et al.* Posttranslational Modifications Mediate the Structural Diversity of Tauopathy Strains. *Cell* (2020) doi:10.1016/j.cell.2020.01.027.
22. Schweighauser, M. *et al.* Cryo-EM structures of tau filaments from the brains of mice transgenic for human mutant P301S Tau. *Acta Neuropathol. Commun.* **11**, 160 (2023).
23. Zhao, W. *et al.* Cryo-EM structures reveal variant Tau amyloid fibrils between the rTg4510 mouse model and sporadic human tauopathies. *Cell Discov.* **10**, 27 (2024).
24. Chen, D. *et al.* FTD-tau S320F mutation stabilizes local structure and allosterically promotes amyloid motif-dependent aggregation. *Nat. Commun.* **14**, 1625 (2023).
25. Joseph, M., Anglada-Huguet, M., Paesler, K., Mandelkow, E. & Mandelkow, E.-M. Anti-aggregant tau mutant promotes neurogenesis. *Mol Neurodegener* **12**, 88 (2017).
26. Pir, G. J. *et al.* Suppressing Tau Aggregation and Toxicity by an Anti-Aggregant Tau Fragment. *Mol Neurobiol* **56**, 3751–3767 (2019).
27. Sydow, A. *et al.* Tau-Induced Defects in Synaptic Plasticity, Learning, and Memory Are Reversible in Transgenic Mice after Switching Off the Toxic Tau Mutant. *J Neurosci* **31**, 2511–2525 (2011).
28. Mocanu, M.-M. *et al.* The Potential for -Structure in the Repeat Domain of Tau Protein Determines Aggregation, Synaptic Decay, Neuronal Loss, and Coassembly with Endogenous Tau in Inducible Mouse Models of Tauopathy. *J Neurosci* **28**, 737–748 (2008).
29. Bergen, M. von *et al.* Mutations of Tau Protein in Frontotemporal Dementia Promote Aggregation of Paired Helical Filaments by Enhancing Local β-Structure. *J Biol Chem* **276**, 48165–48174 (2001).
30. Nixon, R. A. Autophagy–lysosomal-associated neuronal death in neurodegenerative disease. *Acta Neuropathol.* **148**, 42 (2024).
31. Ihara, Y., Morishima-Kawashima, M. & Nixon, R. The Ubiquitin–Proteasome System and the Autophagic–Lysosomal System in Alzheimer Disease. *Cold Spring Harb. Perspect. Med.* **2**, a006361 (2012).
32. Keller, J. N., Hanni, K. B. & Markesbery, W. R. Impaired Proteasome Function in Alzheimer's Disease. *J. Neurochem.* **75**, 436–439 (2000).
33. Bobkova, N. V. *et al.* Therapeutic Effect of Exogenous Hsp70 in Mouse Models of Alzheimer's Disease. *J. Alzheimer's Dis.* **38**, 425–435 (2014).
34. Voss, K., Combs, B., Patterson, K. R., Binder, L. I. & Gamblin, T. C. Hsp70 Alters Tau Function and Aggregation in an Isoform Specific Manner. *Biochemistry* **51**, 888–898 (2012).
35. Nachman, E. *et al.* Disassembly of Tau fibrils by the human Hsp70 disaggregation machinery generates small seeding-competent species. *J Biol Chem* **295**, 9676–9690 (2020).
36. Young, Z. T. *et al.* Stabilizing the Hsp70-Tau Complex Promotes Turnover in Models of Tauopathy. *Cell Chem. Biol.* **23**, 992–1001 (2016).
37. Fontaine, S. N. *et al.* The active Hsc70/tau complex can be exploited to enhance tau turnover without damaging microtubule dynamics. *Hum Mol Genet* **24**, 3971–3981 (2015).

38. Fontaine, S. N. *et al.* Isoform-selective Genetic Inhibition of Constitutive Cytosolic Hsp70 Activity Promotes Client Tau Degradation Using an Altered Co-chaperone Complement*. *J Biol Chem* **290**, 13115–13127 (2015).
39. Yang, X. & Tohda, C. Heat Shock Cognate 70 Inhibitor, VER-155008, Reduces Memory Deficits and Axonal Degeneration in a Mouse Model of Alzheimer's Disease. *Front. Pharmacol.* **9**, 48 (2018).
40. Jinwal, U. K. *et al.* Chemical Manipulation of Hsp70 ATPase Activity Regulates Tau Stability. *J Neurosci* **29**, 12079–12088 (2009).
41. Yu, A. *et al.* Tau protein aggregates inhibit the protein-folding and vesicular trafficking arms of the cellular proteostasis network. *J Biol Chem* **294**, 7917–7930 (2019).
42. Thompson, A. D. *et al.* Analysis of the Tau-Associated Proteome Reveals That Exchange of Hsp70 for Hsp90 Is Involved in Tau Degradation. *ACS Chem. Biol.* **7**, 1677–1686 (2012).
43. Dickey, C. A. *et al.* The high-affinity HSP90-CHIP complex recognizes and selectively degrades phosphorylated tau client proteins. *J Clin Invest* **117**, 648–658 (2007).
44. Salminen, A., Ojala, J., Kaarniranta, K., Hiltunen, M. & Soininen, H. Hsp90 regulates tau pathology through co-chaperone complexes in Alzheimer's disease. *Prog Neurobiol* **93**, 99–110 (2011).
45. Moll, A. *et al.* Hsp multichaperone complex buffers pathologically modified Tau. *Nat Commun* **13**, 3668 (2022).
46. Karagöz, G. E. *et al.* Hsp90-Tau Complex Reveals Molecular Basis for Specificity in Chaperone Action. *Cell* **156**, 963–974 (2014).
47. Cook, C. *et al.* Loss of HDAC6, a novel CHIP substrate, alleviates abnormal tau accumulation. *Hum Mol Genet* **21**, 2936–45 (2012).
48. Dickey, C. A. *et al.* Akt and CHIP coregulate tau degradation through coordinated interactions. *P Natl Acad Sci Usa* **105**, 3622–7 (2008).
49. Weickert, S., Wawrzyniuk, M., John, L. H., Rüdiger, S. G. D. & Drescher, M. The mechanism of Hsp90-induced oligomerizaton of Tau. *Sci Adv* **6**, eaax6999 (2020).
50. Rutledge, B. S., Choy, W.-Y. & Duennwald, M. L. Folding or holding?—Hsp70 and Hsp90 chaperoning of misfolded proteins in neurodegenerative disease. *J. Biol. Chem.* **298**, 101905 (2022).
51. Jinwal, U. K. *et al.* Imbalance of Hsp70 family variants fosters tau accumulation. *FASEB J.* **27**, 1450–1459 (2013).
52. Miyata, Y. *et al.* Cysteine Reactivity Distinguishes Redox Sensing by the Heat-Inducible and Constitutive Forms of Heat Shock Protein 70. *Chem. Biol.* **19**, 1391–1399 (2012).
53. Martin, M. D. *et al.* Inhibition of Both Hsp70 Activity and Tau Aggregation in Vitro Best Predicts Tau Lowering Activity of Small Molecules. *Acs Chem Biol* **11**, 2041–2048 (2016).
54. Jinwal, U. K. *et al.* Hsp70 ATPase Modulators as Therapeutics for Alzheimer's and other Neurodegenerative Diseases. *Mol. Cell. Pharmacol.* **2**, 43–46 (2010).
55. Massey, A. J. *et al.* A novel, small molecule inhibitor of Hsc70/Hsp70 potentiates Hsp90 inhibitor induced apoptosis in HCT116 colon carcinoma cells. *Cancer Chemother. Pharmacol.* **66**, 535–545 (2010).
56. Farizatto, K. L. G., Almeida, M. F., Long, R. T. & Bahr, B. A. Early Synaptic Alterations and Selective Adhesion Signaling in Hippocampal Dendritic Zones Following Organophosphate Exposure. *Sci. Rep.* **9**, 6532 (2019).
57. Almeida, M. F. *et al.* Distinct and dementia related synaptopathy in the hippocampus after military blast exposures. *Brain Pathol.* **31**, e12936 (2021).

58. McKenna, M. *et al.* Organotypic whole hemisphere brain slice models to study the effects of donor age and oxygen-glucose-deprivation on the extracellular properties of cortical and striatal tissue. *J. Biol. Eng.* **16**, 14 (2022).
59. Bahr, B. A. *et al.* Amyloid β protein is internalized selectively by hippocampal field CA1 and causes neurons to accumulate amyloidogenic carboxyterminal fragments of the amyloid precursor protein. *J. Comp. Neurol.* **397**, 139–147 (1998).
60. Caba, E. *et al.* Excitotoxic stimulation activates distinct pathogenic and protective expression signatures in the hippocampus. *J. Cell. Mol. Med.* **25**, 9011–9027 (2021).
61. Farizatto, K. L. G., Ikonne, U. S., Almeida, M. F., Ferrari, M. F. R. & Bahr, B. A. Aβ42-mediated proteasome inhibition and associated tau pathology in hippocampus are governed by a lysosomal response involving cathepsin B: Evidence for protective crosstalk between protein clearance pathways. *PLoS ONE* **12**, e0182895 (2017).

Bryan et al., Figure 1.

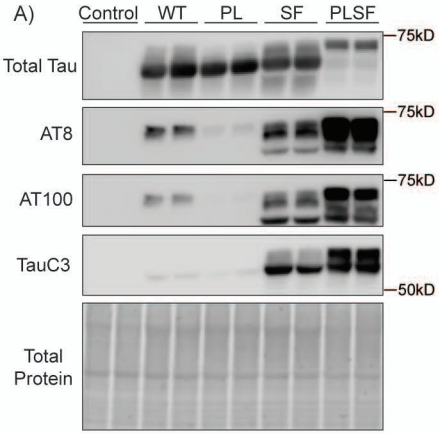

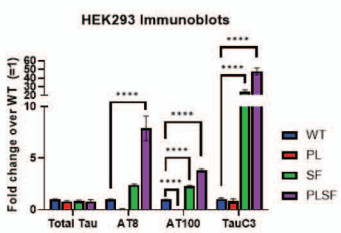

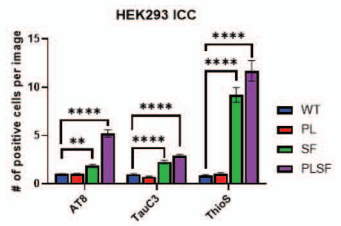

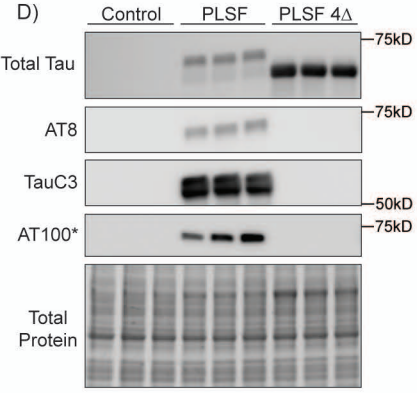

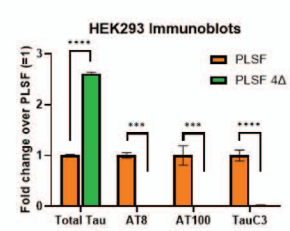

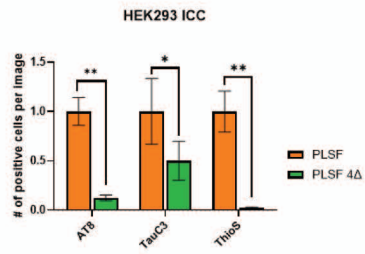

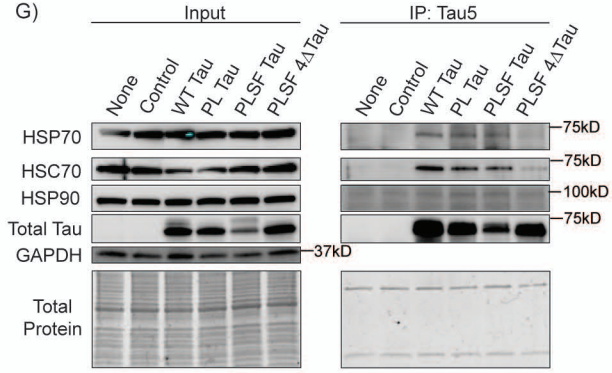

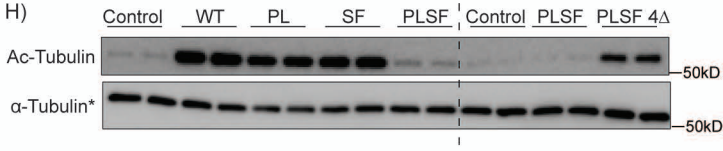

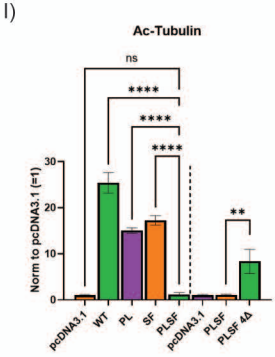

Bryan et al., Figure 2.

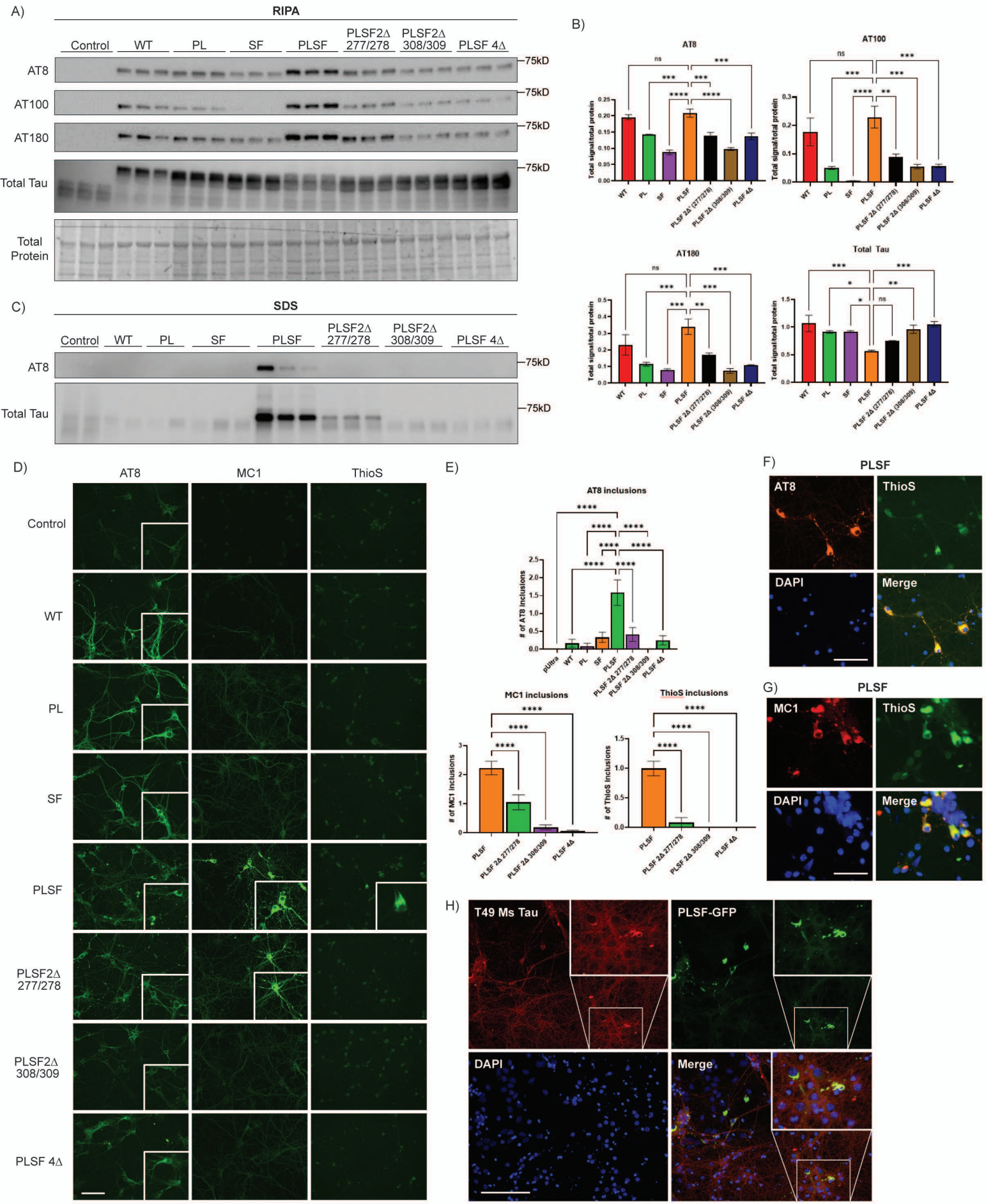

Bryan et al., Figure 3.

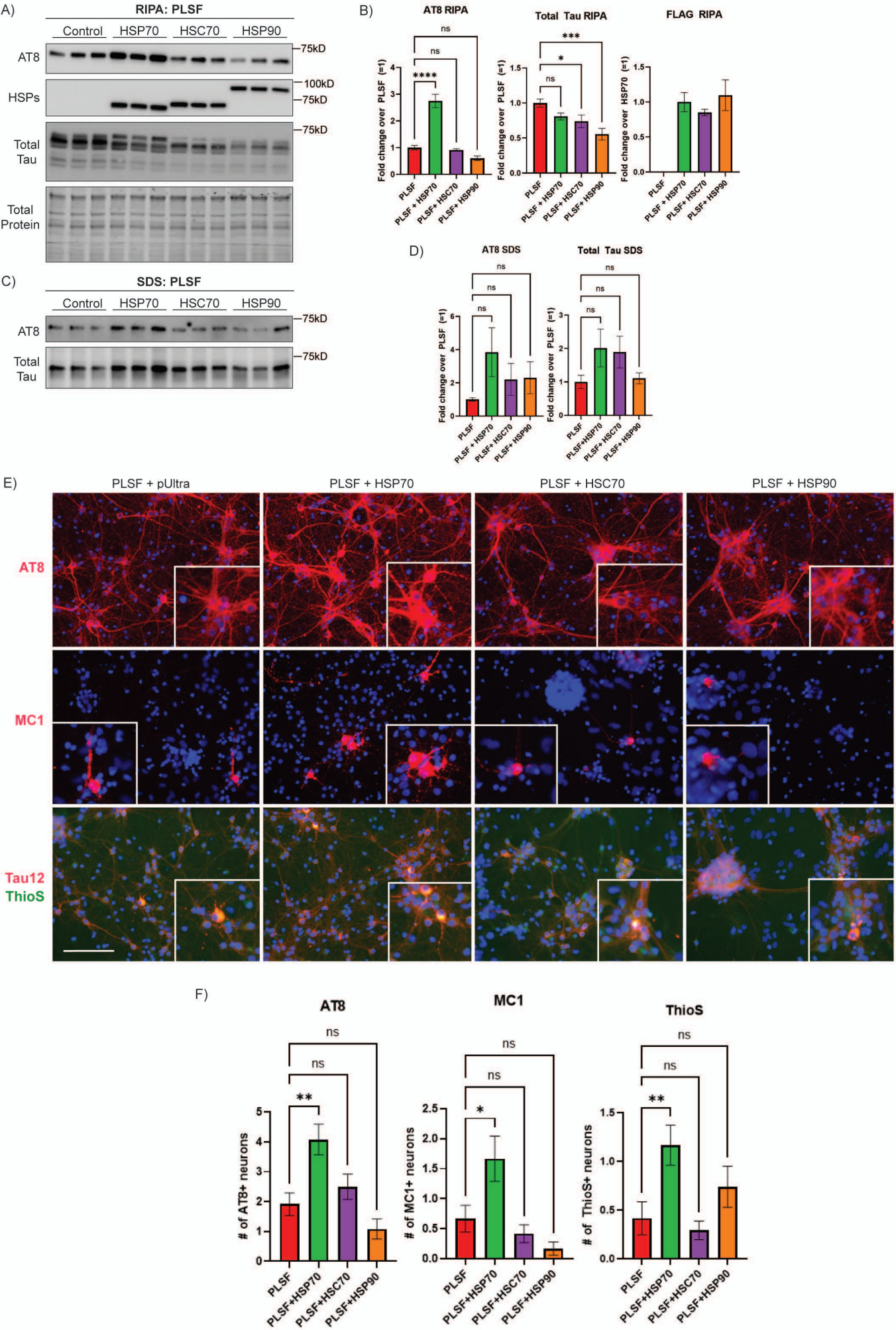

Bryan et al., Figure 4.

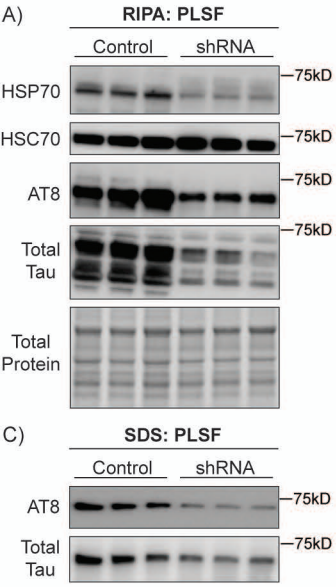

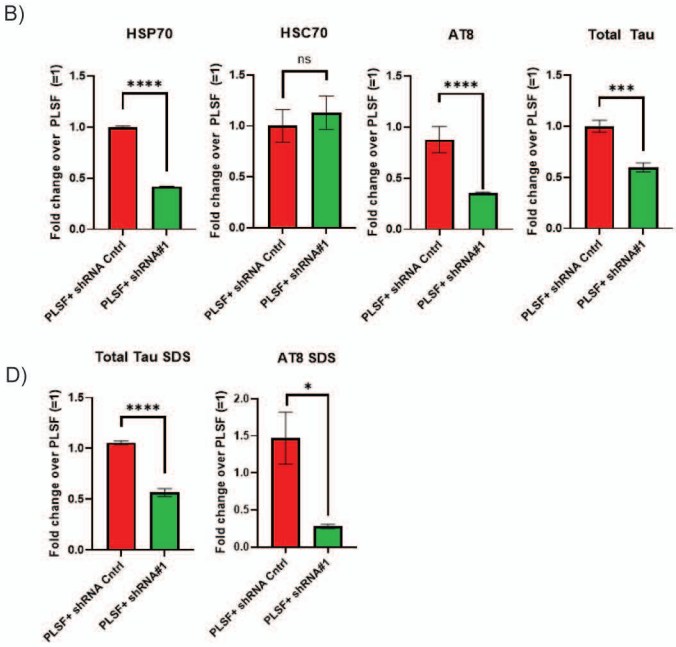

Bryan et al., Figure 5.

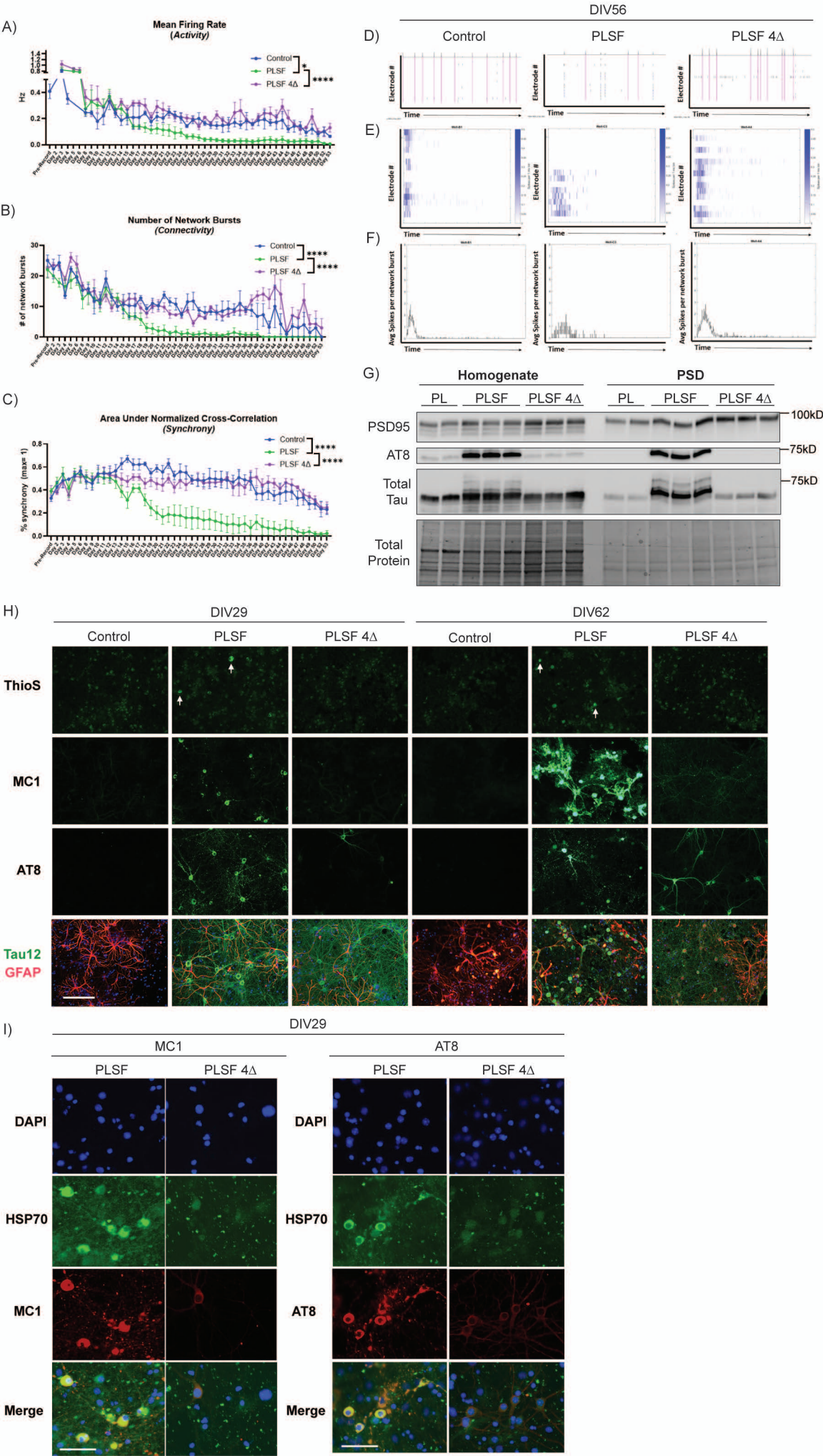
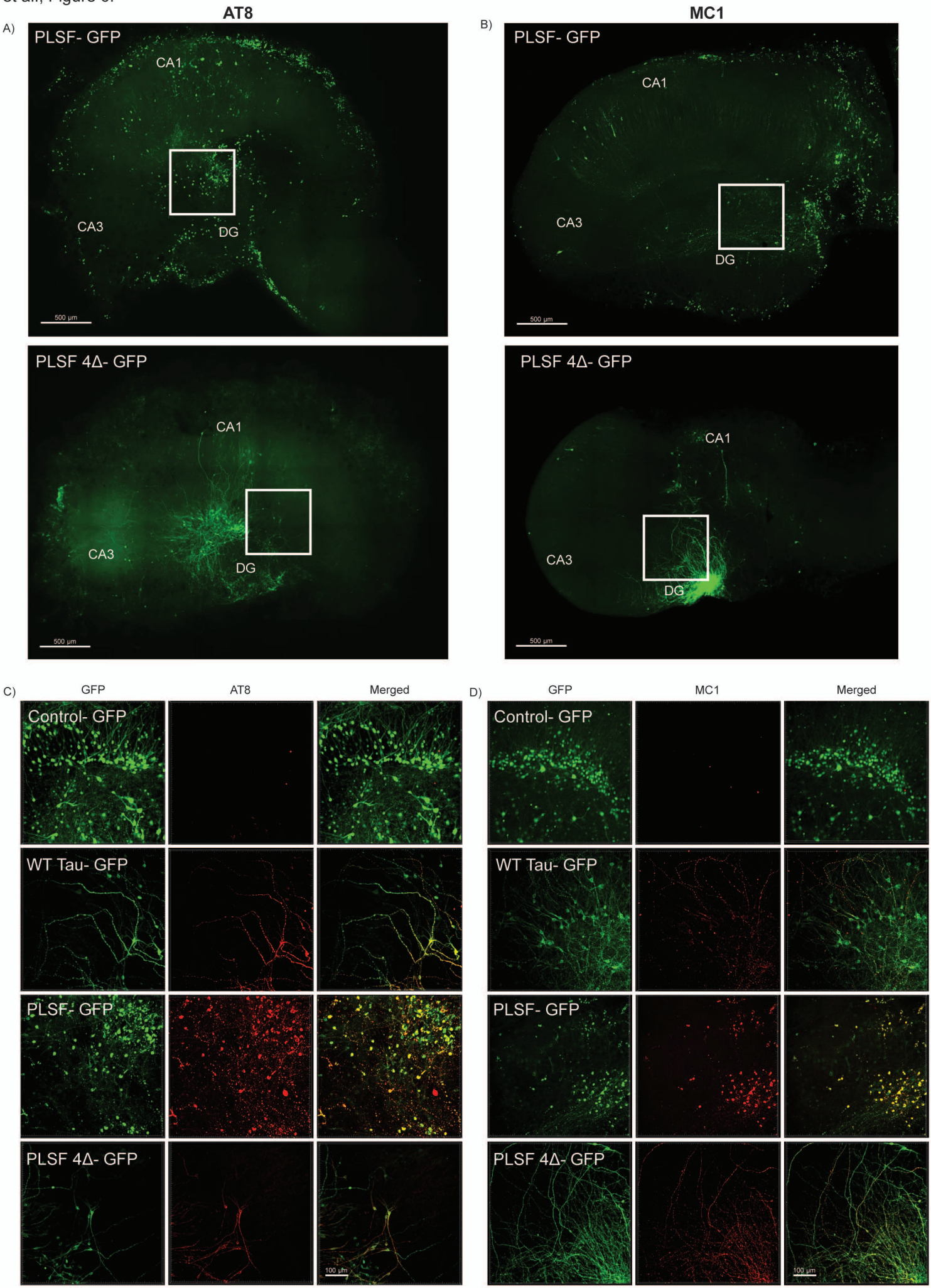
Bryan et al., Figure 6.